Cell Research (2017) 27:1100-1114.

www.nature.com/cr

ORIGINAL ARTICLE

Mettl3-mediated m^{6}A regulates spermatogonial differentiation and meiosis initiation

Kai Xu[1, 5, *], Ying Yang[2, *], Gui-Hai Feng[1, *], Bao-Fa Sun[2, *], Jun-Qing Chen[1, 3, *], Yu-Fei Li[1, 5], Yu-Sheng Chen[2, 5], Xin-Xin Zhang[1, 5], Chen-Xin Wang[1, 5], Li-Yuan Jiang[1, 5], Chao Liu[1, 5], Ze-Yu Zhang[4, 5], Xiu-Jie Wang[4, 5], Qi Zhou[1, 5], Yun-Gui Yang[2, 5], Wei Li[1, 5]

[1]State Key Laboratory of Stem Cell and Reproductive Biology, Institute of Zoology, Chinese Academy of Sciences, Beijing 100101, China; [2]Key Laboratory of Genomic and Precision Medicine, Collaborative Innovation Center of Genetics and Development, CAS Center for Excellence in Molecular Cell Science, Beijing Institute of Genomics, Chinese Academy of Sciences, Beijing 100101, China; [3]State Key Laboratory of Reproductive Medicine, Department of Histology and Embryology, Nanjing Medical University, Nanjing, Jiangsu 210029, China; [4]Key Laboratory of Genetic Network Biology, Collaborative Innovation Center of Genetics and Development, Institute of Genetics and Developmental Biology, Chinese Academy of Sciences, Beijing 100101, China; [5]University of Chinese Academy of Sciences, Beijing 100049, China

METTL3 catalyzes the formation of N^6-methyl-adenosine (m^{6}A) which has important roles in regulating various biological processes. However, the *in vivo* function of *Mettl3* remains largely unknown in mammals. Here we generated germ cell-specific *Mettl3* knockout mice and demonstrated that *Mettl3* was essential for male fertility and spermatogenesis. The ablation of *Mettl3* in germ cells severely inhibited spermatogonial differentiation and blocked the initiation of meiosis. Transcriptome and m^{6}A profiling analysis revealed that genes functioning in spermatogenesis had altered profiles of expression and alternative splicing. Our findings provide novel insights into the function and regulatory mechanisms of Mettl3-mediated m^{6}A modification in spermatogenesis and reproduction in mammals.

***Keywords*:** *Mettl3*; m^{6}A; spermatogenesis; spermatogonial differentiation; meiosis; alternative splicing
Cell Research (2017) **27**:1100-1114. doi: 10.1038/cr.2017.100; published online 15 August 2017

Introduction

Over 100 types of RNA modifications have been identified in mRNAs and non-coding RNAs, among which the N^6-methyl-adenosine (m^{6}A) is the most prevalent mRNA modification in eukaryotes [1]. m^{6}A formation is catalyzed by the RNA methyltransferase complex containing methyltransferase like 3 (METTL3), METTL14 and Wilms' tumor 1-associating protein (WTAP) [2-6]. m^{6}A is a reversible modification that can be erased by demethylases, fat-mass and obesity-associated protein (FTO) and α-ketoglutarate-dependent dioxygenase alkB homolog 5 (ALKBH5) [7, 8], and recognized by YTH-domain containing family 'reader' proteins [9-13]. m^{6}A modification mediates a variety of RNA processing steps, and thus regulates mRNA splicing [11], mRNA stability [9], translation efficiency [10, 12-15], microRNA processing [16, 17] and XIST-mediated transcriptional repression [18]. Recent studies revealed m^{6}A modulation of mRNA expression to be involved in obesity [19], the circadian clock [20], and the DNA damage response [21]. Additionally, it also plays important roles in a variety of biological processes including pluripotency maintenance of stem cells [22-24], the maternal-to-zygotic transition [25], sex determination [26, 27] and plant shoot stem cell fate determination [28]. As the key 'writer' of m^{6}A modification, *Mettl3* has been demonstrated to modulate neuronal functions and sex determination in *Drosophila* and regulate early embryonic development and stem cell pluripotency in mice [22-24, 26, 27]. However, due to the early lethality of *Mettl3* knockout mice [24], the *in vivo* biological functions of *Mettl3*-mediated m^{6}A modification in mammalian tissue development remain to be

*These five authors contributed equally to this work.
Correspondence: Wei Li[a], Yun-Gui Yang[b], Qi Zhou[c]
[a]E-mail: liwei@ioz.ac.cn
[b]E-mail: ygyang@big.ac.cn
[c]E-mail: qzhou@ioz.ac.cn
Received 14 June 2017; revised 27 June 2017; accepted 20 July 2017; published online 15 August 2017

elucidated.

Here, we generated germ cell conditional *Mettl3* knockout mice and found that *Mettl3* regulates spermatogonial differentiation and meiosis and is essential for male fertility and spermatogenesis. Mechanistically, we found that METTL3-mediated m^{6}A modification regulates the alternative splicing of genes functioning in spermatogenesis and the global gene expression pattern in testes.

Results

Mettl3 is essential for male fertility and spermatogonial differentiation during spermatogenesis

To explore the function of *Mettl3* in mouse spermatogenesis, we first used immunostaining to examine the expression of METTL3 in the mouse testis at 6 and 12 days post-partum (P6 and P12). METTL3 was expressed in both germ cells and somatic cells during testis development (Supplementary information, Figure S1A). Furthermore, METTL3 expression was relatively higher in undifferentiated spermatogonia that expressed PLZF (promyelocytic leukemia zinc-finger protein) at P6 (Supplementary information, Figure S1B). To investigate the function of *Mettl3*-mediated m^{6}A modification in gametogenesis in mice, we specifically knocked out the *Mettl3* gene in the germ cells. Using CRISPR-Cas9 system-assisted homologous recombination, two loxp sites were inserted into the intron 1 and intron 4 of the *Mettl3* gene to generate mice carrying the floxed allele (*Mettl3*$^{flox/+}$) (Supplementary information, Figure S1C). To disrupt the *Mettl3* gene in germ cells, the *Mettl3*$^{flox/+}$ mice were further mated with the *Vasa-Cre* mice that specifically expressed the Cre recombinase in germ cells driven by a *Vasa* promoter as early as embryonic day 15.5 (E15.5) [29] (Supplementary information, Figure S1C). Six genotypes of *Mettl3* allele, including *Mettl3*$^{+/+}$, *Mettl3*$^{flox/+}$, *Mettl3*$^{flox/flox}$, *Vasa-Cre*, *Mettl3*$^{flox/+}$*Vasa-Cre* and *Mettl3*$^{flox/-}$ *Vasa-Cre*, were obtained and verified by PCR and Sanger sequencing (Supplementary information, Figure S1D-S1H). The *Mettl3*$^{flox/-}$*Vasa-Cre* mice showed specific deletion of exons 2~4 and loss of METTL3 expression in PLZF-positive spermatogonia, confirming the conditional knockout of *Mettl3* (referred as *Mettl3*^{cKO}) (Figure 1A and Supplementary information, Figure S1E, S1H). The *Mettl3*$^{+/+}$, *Mettl3*$^{flox/+}$, *Mettl3*$^{flox/flox}$, *Vasa-Cre* and *Mettl3*$^{flox/+}$*Vasa-Cre* mice were healthy and phenotypically normal, and were used as control in the following experiments (referred as *Mettl3*^{Ctrl}).

Next, we analyzed the phenotypes of the *Mettl3*^{cKO} mice. The *Mettl3*^{cKO} mice were normal in growth, but were completely infertile and had much smaller testes with 80% reduction in testis weight at 8 weeks (Figure 1B and 1C). Rare differentiated cell types of spermatocytes were observed in the *Mettl3*^{cKO} seminiferous tubules at P8, P10 and P12, and no spermatids were observed at 8 weeks by hematoxylin and eosin (H&E) staining, indicating a severe defect in spermatogenesis in the *Mettl3*^{cKO} mice (Figure 1D). Co-staining of the germ cell marker DDX4 and the undifferentiated spermatogonia marker PLZF showed the presence of undifferentiated spermatogonia that were normal, but the number of germ cells was significantly reduced in the *Mettl3*^{cKO} testes at P8, P10 and P12 (Figure 1E, 1F and Supplementary information, Figure S1I-S1L). We next traced advanced stages of spermatogonial differentiation using the differentiated spermatogonial cell marker KIT at P8, the initial stage of spermatogonial differentiation, and P12. KIT-positive cells were significantly reduced in the *Mettl3*^{cKO} testes at both P8 and P12 (Figure 1G-1J). Collectively, these results demonstrated that *Mettl3* is essential for male fertility in mice and its deletion leads to defects in the initiation of spermatogonial differentiation.

Mettl3 deletion causes a severe defect in meiosis during spermatogenesis

Meiosis, as the key feature of spermatogenesis, initiates around P10 and spermatocytes enter meiotic prophase around P12. To investigate the function of Mettl3 in meiosis, we examined the expression of meiotic marker genes at P10 and P12 by immunostaining. STRA8, a marker of meiosis initiation, showed a much-reduced expression level in *Mettl3*^{cKO} testes at P10 and P12. Both the ratio of STRA8-positive seminiferous tubules and the number of STRA8-expressing cells per tubule were significantly reduced in *Mettl3*^{cKO} testes compared to *Mettl3*^{Ctrl} testes at P10 and P12 (Figure 2A). The number of cells expressing the synaptonemal complex component SYCP3 in *Mettl3*^{cKO} testes was also much less than that in *Mettl3*^{Ctrl} testes (Figure 2B). We next traced the progression of meiotic prophase that can be divided into leptotene, zygotene, pachytene stages according to the distribution patterns of SYCP3 and γH2AX in spermatocyte nuclear spreads. Pachytene-stage spermatocytes were only detectable in *Mettl3*^{Ctrl} mice and not in *Mettl3*^{cKO} mice, while leptotene- and zygotene/zygotene-like-stage spermatocytes were observed in both *Mettl3*^{Ctrl} and *Mettl3*^{cKO} mice (Figure 2C-2E and Supplementary information, Figure S2A). *Mettl3*^{Ctrl} testes had around 29%, 31% and 40% of spermatocytes at the leptotene, zygotene and pachytene stages, respectively, whereas 84% of spermatocytes in *Mettl3*^{cKO} testes were in the zygotene/zygotene-like stage but none were in pachytene (Figure 2F).

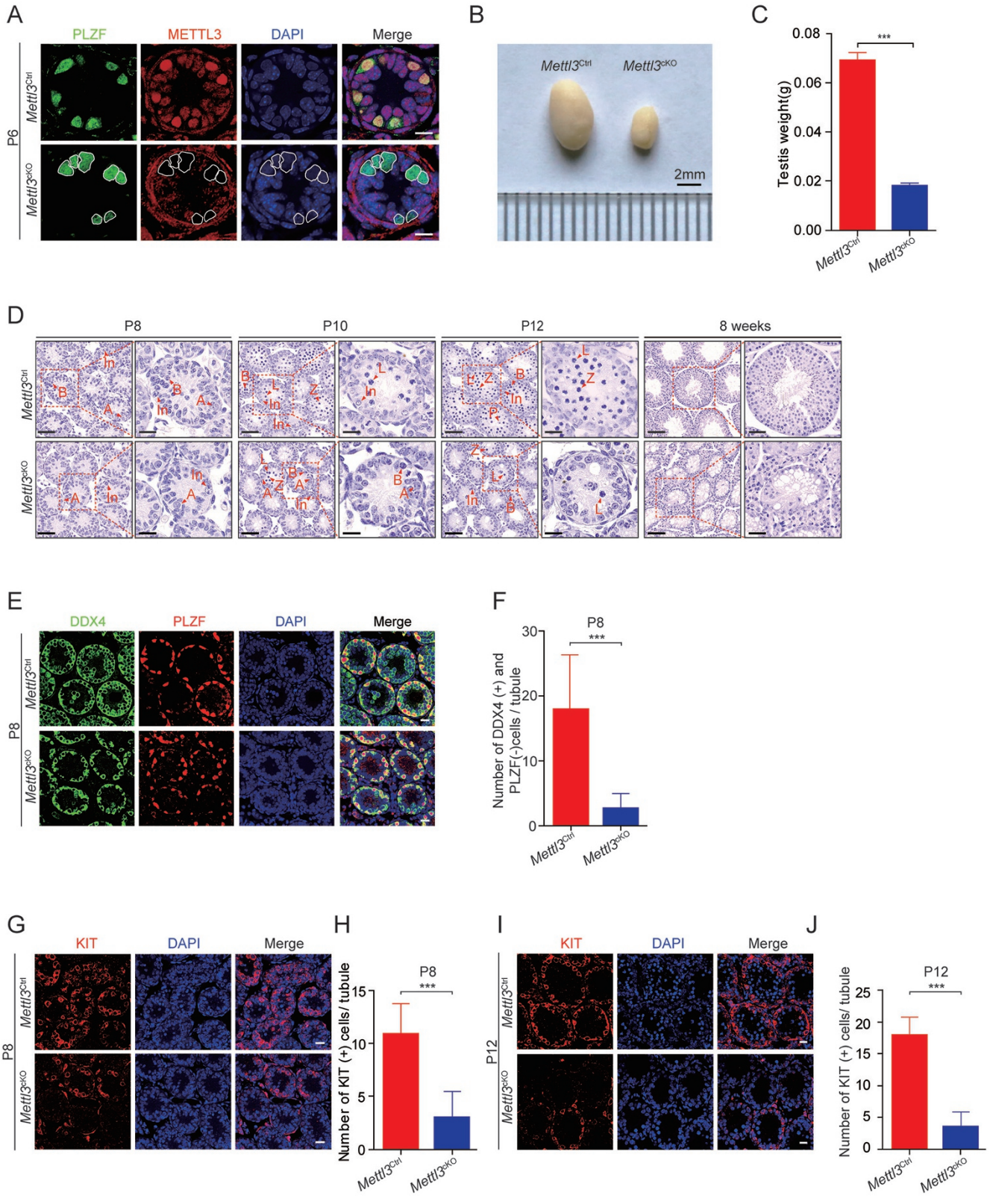
A
PLZF
METTL3
DAPI
Merge
P6
Mettl3Ctrl
Mettl3cKO
B
Mettl3Ctrl
Mettl3cKO
2mm
C
Testis weight(g)
0.08
0.06
0.04
0.02
0.00
***
Mettl3Ctrl
Mettl3cKO
D
P8
P10
P12
8 weeks
Mettl3Ctrl
Mettl3cKO
In
B
A
L
Z
P
E
DDX4
PLZF
DAPI
Merge
P8
Mettl3Ctrl
Mettl3cKO
F
P8
***
Number of DDX4 (+) and PLZF(-)cells / tubule
30
20
10
0
Mettl3Ctrl
Mettl3cKO
G
KIT
DAPI
Merge
P8
Mettl3Ctrl
Mettl3cKO
H
P8
***
Number of KIT (+) cells/ tubule
15
10
5
0
Mettl3Ctrl
Mettl3cKO
I
KIT
DAPI
Merge
P12
Mettl3Ctrl
Mettl3cKO
J
P12
***
Number of KIT (+) cells/ tubule
25
20
15
10
5
0
Mettl3Ctrl
Mettl3cKO

To confirm the blockage of meiosis at the zygotene/zygotene-like stage, we examined testes for the presence of additional marker proteins. We found that the synapsis marker SYCP1 was also not detected in *Mettl3*^{cKO} spermatocytes (Supplementary information, Figure S2B). In contrast to the much greater number of foci of the DSB repair protein RAD51 at the zygotene/zygotene-like stage in *Mettl3*^{Ctrl} spermatocytes, very few RAD51 foci were detected in *Mettl3*^{cKO} spermatocytes, indicating defective DSB repair during meiosis upon *Mettl3* knockout (Figure 2C-2E). γH2AX expression is strong at the leptotene stage (referred to as positive), gradually decreases around the zygotene stage (referred to as partial positive), and the protein is enriched in the sex-body at the pachytene stage (referred as only sex-body positive). While all three expression patterns could be seen in nuclear spreads of *Mettl3*^{Ctrl} spermatocytes, the only sex-body-positive pattern was not observed in *Mettl3*^{cKO} nuclear spreads (Figure 2G and Supplementary information, Figure S2C). Spermatocytes blocked in meiosis will undergo apoptosis; this was detectable by TUNEL assays showing a significantly increased apoptotic signal in *Mettl3*^{cKO} testes at P12 (Figure 2H and 2I). These results demonstrate that *Mettl3*-deficient spermatocytes are unable to reach the pachytene stage of meiotic prophase and that *Mettl3* is required for normal meiosis.

Mettl3 deletion alters expression pattern of spermatogenesis-related genes

To systematically illuminate gene expression changes resulting from the *Mettl3* conditional knockout in spermatogenesis, we compared the transcriptome between *Mettl3*^{Ctrl} and *Mettl3*^{cKO} testes at P6 and P12 through high-throughput RNA sequencing. The correlation analysis showed that the expression of the majority of genes in testes was not influenced by *Mettl3* deletion (Supplementary information, Figure S3A, S3B and Table S4). We found that a total of 258 genes were differentially expressed in the *Mettl3*^{cKO} testes at P6. These included 157 down-regulated genes that were significantly enriched in genes required for the regulation of spermatogenesis including the meiotic cell cycle and synaptonemal complex assembly (Supplementary information, Figure S3C). We found that 941 genes were differentially expressed in *Mettl3*^{cKO} testes at P12. These included 699 down-regulated genes that were mainly enriched in genes required for spermatogenesis and regulation of meiosis (Figure 3A and Supplementary information, Table S4). We next examined expression patterns of 50 genes specifically expressed in germ cells according to a previous study [30]. Unsupervised cluster analysis showed that the *Mettl3*^{cKO} expression pattern at P12 was much more similar to *Mettl3*^{Ctrl} at P6 than *Mettl3*^{Ctrl} at P12, consistent with the severely impaired spermatogonial differentiation observed in *Mettl3*^{cKO} testes (Figures 3B, 3C and Supplementary information, Table S4). Genes with reported functions in spermatogenesis [31-33] were mapped into an interaction network to illustrate regulationary relationships by Pathway Studio (Figure 3D). The genes significantly down-regulated in *Mettl3*^{cKO} testes included 9 genes involved in spermatogonial stem cell maintenance (*Dazl*, *Ddx4*, *Plzf*, *Pax7*, *Nanos2*, *Id4*, *Pou3f1*, *Taf4b*, *Bcl6*); 6 genes in spermatogonial differentiation (*Sohlh1*, *Sohlh2*, *Neurog3*, *Kit*, *Dmrt1*, *Sox3*); 8 genes in cell cycle (*Ccna1*, *Ccna2*, *Ccnb1*, *Ccnb2*, *Ccnb3*, *Ccne2*, *Cdk1*, *Rad51*); and 9 genes in meiosis (*Stra8*, *Sycp1*, *Sycp3*, *Spo11*, *Rad18*, *Dmc1*, *Rec8*, *Mlh1*, *Smc1b*) (Figure 3E, 3F and Supplementary information,

Figure 1 *Mettl3* is essential for male fertility and spermatogonial differentiation during spermatogenesis. **(A)** Confocal immunofluorescence detection of METTL3 by staining of the *Mettl3*^{Ctrl} and *Mettl3*^{cKO} testes at postnatal day 6 (P6). PLZF was co-stained to indicate the location of the undifferentiated spermatogonia. The DNA was stained with DAPI. White circles denote the *Mettl3* null spermatogonia. Scale bar, 10 μm. **(B)** Morphological analysis of the 8-week-old *Mettl3*^{Ctrl} and *Mettl3*^{cKO} testes. Scale bar, 2 mm. **(C)** Testis weight of the 8-week-old *Mettl3*^{Ctrl} and *Mettl3*^{cKO} mice. Student's *t*-test, error bars indicate standard error of measurement (SEM). ***P < 0.001, n = 8. **(D)** Hematoxylin eosin (H&E) staining of *Mettl3*^{Ctrl} and *Mettl3*^{cKO} testes at postnatal day 8 (P8), postnatal day 10 (P10), postnatal day 12 (P12) and 8 weeks showed that the spermatogonial differentiation was inhibited in *Mettl3* knockout testes. Red arrows indicate the representative stages of the spermatocytes. A, type A spermatogonia; In, intermediate spermatogonia; B, type B spermatogonia; L, leptotene spermatocytes; Z, zygotene spermatocytes; P, pachytene spermatocytes. Left panel, P8, P10, P12, scale bar, 20 μm; 8 weeks, scale bar, 100 μm. Right panel, P8, P10, P12, scale bar, 5 μm; 8 weeks, scale bar, 20 μm. **(E)** Immunofluorescence co-staining of PLZF and DDX4 in *Mettl3*^{Ctrl} and *Mettl3*^{cKO} testes at P8. Scale bar, 20 μm. **(F)** Statistics results of DDX4-positive but PLZF-negative cells in *Mettl3*^{Ctrl} and *Mettl3*^{cKO} testes at P8. At least 100 tubules were counted from 3 different mice. Student's *t*-test, error bars indicate SEM. ***P < 0.001. **(G)** Immunofluorescence staining of KIT in *Mettl3*^{Ctrl} and *Mettl3*^{cKO} testes at P8. Scale bar, 20 μm. **(H)** Statistics of Kit-positive cells in *Mettl3*^{Ctrl} and *Mettl3*^{cKO} testes at P8. At least 100 tubules were counted from three different mice. Student's *t*-test, error bars indicate SEM. ***P < 0.001. **(I)** Immunofluorescence staining of KIT in *Mettl3*^{Ctrl} and *Mettl3*^{cKO} testes at P12. Scale bar, 20 μm. **(J)** Statistics of KIT-positive cells in *Mettl3*^{Ctrl} and *Mettl3*^{cKO} testes at P12. At least 100 tubules were counted from 3 different mice. Student's *t*-test, error bars indicate SEM. ***P < 0.001.

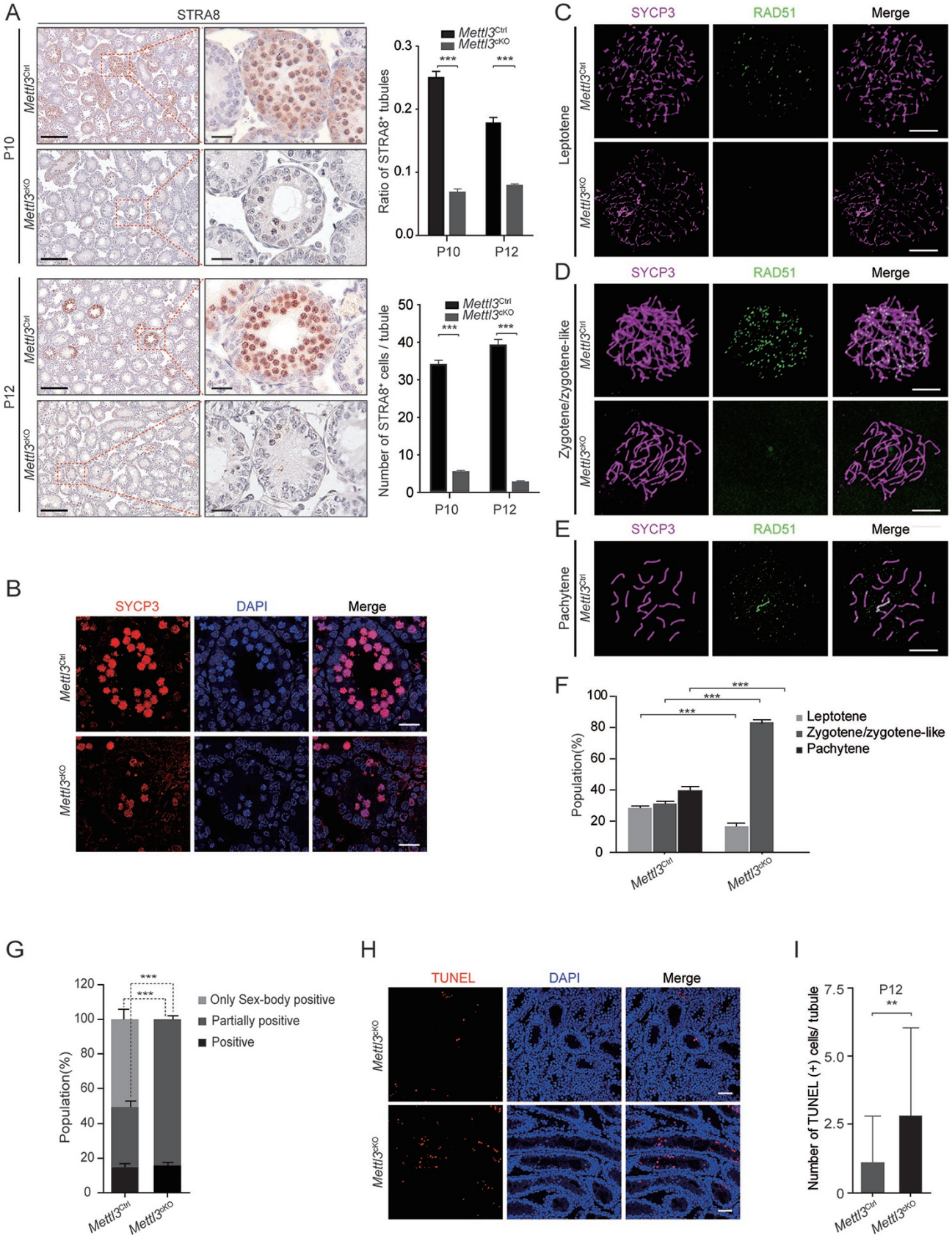
A
STRA8
P10
P12
Mettl3Ctrl
Mettl3cKO
Ratio of STRA8+ tubules
Number of STRA8+ cells / tubule
P10
P12
B
SYCP3
DAPI
Merge
C
SYCP3
RAD51
Merge
Leptotene
D
Zygotene/zygotene-like
E
Pachytene
F
Population(%)
Leptotene
Zygotene/zygotene-like
Pachytene
G
Only Sex-body positive
Partially positive
Positive
H
TUNEL
DAPI
Merge
I
Number of TUNEL (+) cells/ tubule
P12

Figure S3D). Taken together, this indicate that the *Mettl3* deficiency globally influenced the expression pattern of spermatogenesis-related genes regulating multiple biological processes including spermatogonial stem cell maintenance, differentiation and meiosis.

Mettl3-mediated m^{6}A regulates alternative splicing of genes functioning in spermatogenesis

Previous studies have shown that m^{6}A could influence biological process through regulating alternative splicing events [11, 19]. We therefore employed rMATS software to analyze the differential alternative splicing events between *Mettl3^{Ctrl}* and *Mettl3^{cKO}* transcriptomes [34]. Among the differential splicing events, we mainly detected exon skipping to be enriched, consistent with previous studies [11, 19] (Figure 4A and Supplementary information, Table S5). Gene ontology analysis revealed that the differentially spliced genes between *Mettl3^{Ctrl}* and *Mettl3^{cKO}* samples at P6 were enriched in those for DNA replication and cell division processes whereas those at P12 were enriched for spermatogenesis (Supplementary information, Figure S4A).

We then detected the m^{6}A sites and explored their distribution in P12 testes of wild-type mice through m^{6}A individual-nucleotide-resolution cross-linking and immunoprecipitation (miCLIP) and sequencing (miCLIP-seq). A total of 12 516 putative m^{6}A residues within 5 092 genes were identified in testes (Supplementary information, Table S6). These sites were enriched in the m^{6}A consensus motif (Figure 4B) and were predominantly distributed in the CDS and 3′ UTR regions, especially near stop codon regions (Figure 4C and 4D). Notably, the average m^{6}A site number was higher in genes with skipped exons (Figure 4E). An alternative exon inclusion level measurement also revealed that genes containing m^{6}A had a lower inclusion level in *Mettl3^{cKO}* samples compared to that in *Mettl3^{Ctrl}* samples whereas genes without m^{6}A modification did not show this tendency (Figure 4F and Supplementary information, Figure S4B). These results are consistent with previous reports showing the role of m^{6}A modification in promoting exon inclusion [11, 19].

Next, we examined differential splicing events between *Mettl3^{Ctrl}* and *Mettl3^{cKO}* samples in spermatogenesis-related genes. Our findings showed that 9 genes had significantly decreased exon inclusion levels in *Mettl3^{cKO}* testes (Figure 4G, 4H and Supplementary information, Figure S4C-S4I). The m^{6}A-RIP-qPCR analysis was used to validate the presence of m^{6}A residues in alternative exons or neighboring regions, and the results supported occurrence of alternative splicing events regulated by m^{6}A (Supplementary information, Figure S4J-S4Q). For example, *Dazl*, essential for spermatogenesis, had a shorter transcript with loss of 17 amino acids next to its RNA recognition motif in *Mettl3^{cKO}* testes (Supplementary information, Figure S4C). Similar splicing events were also found in *Sohlh1* regulating spermatogonial stem cell differentiation [35-37], and *Nasp*- and *Cdk11b*-regulating cell division [38-41] (Figure 4I and Supplementary information, Figure S4D, S4E). Taken together, these data revealed that *Mettl3*-mediated m^{6}A modification regulates the alternative splicing of genes that function in spermatogenesis.

Discussion

m^{6}A is the most abundant modification in RNA molecules in eukaryotes and is catalyzed by one of the 'writer' proteins, METTL3 [2-6]. Although several biological functions of *Mettl3*-mediated m^{6}A methylation have been revealed in *Drosophila,* mouse early embryos and embryonic stem cells [22-24, 26, 27], the *in vivo* function in

Figure 2 *Mettl3* deletion causes a severe defect in meiosis during spermatogenesis. **(A)** Immunohistochemical staining of STRA8 in *Mettl3^{Ctrl}* and *Mettl3^{cKO}* testes at P10 and P12. Left panel, scale bar, 100 μm. Right panel, scale bar, 5 μm. Statistics of the ratio of STRA8-positive tubule in *Mettl3^{Ctrl}* and *Mettl3^{cKO}* testes at P10 and P12. At least 750 tubules were counted from 3 different mice. Student's *t*-test, error bars indicate SEM. ***P < 0.001. Statistics of the number of STRA8-positive cells per tubule in *Mettl3^{Ctrl}* and *Mettl3^{cKO}* testes at P10 and P12. At least 50 tubules were counted from 3 different mice. Student's *t*-test, error bars indicate SEM. ***P < 0.001. **(B)** Immunofluorescence staining of SYCP3 in *Mettl3^{Ctrl}* and *Mettl3^{cKO}* testes at P12. DNA was stained with DAPI. Scale bar, 20 μm. **(C-E)** Immunofluorescence staining for detection of SYCP3 and RAD51 on nuclear surface spreads of leptotene **(C)**, zygotene-like **(D)** and pachytene **(E)** spermatocytes from *Mettl3^{Ctrl}* and *Mettl3^{cKO}* testes at P12. Scale bar, 5 μm. **(F)** Statistics of the proportion of leptotene, zygotene/zygotene-like, pachytene spermatocytes in *Mettl3^{Ctrl}* and *Mettl3^{cKO}* testes at P12. At least 1 000 cells were counted from 3 different mice. Student's *t*-test, error bars indicate SEM. ***P < 0.001. **(G)** Statistics of the proportion of γ-H2AX expression patterns including only sex-body positive, partially positive and positive in *Mettl3^{Ctrl}* and *Mettl3^{cKO}* spermatocytes at P12. At least 550 cells were counted from 3 different mice. Student's *t*-test, error bars indicate SEM. ***P < 0.001. **(H)** Immunofluorescence staining of TUNEL in *Mettl3^{Ctrl}* and *Mettl3^{cKO}* testes at P12. The DNA was stained with DAPI. Scale bar, 50 μm. **(I)** Statistics of number of TUNEL-positive cells per tubule in *Mettl3^{Ctrl}* and *Mettl3^{cKO}* testes at P12. At least 50 tubules were counted from 3 different mice. Student's *t*-test, error bars indicate SEM. **P < 0.01.

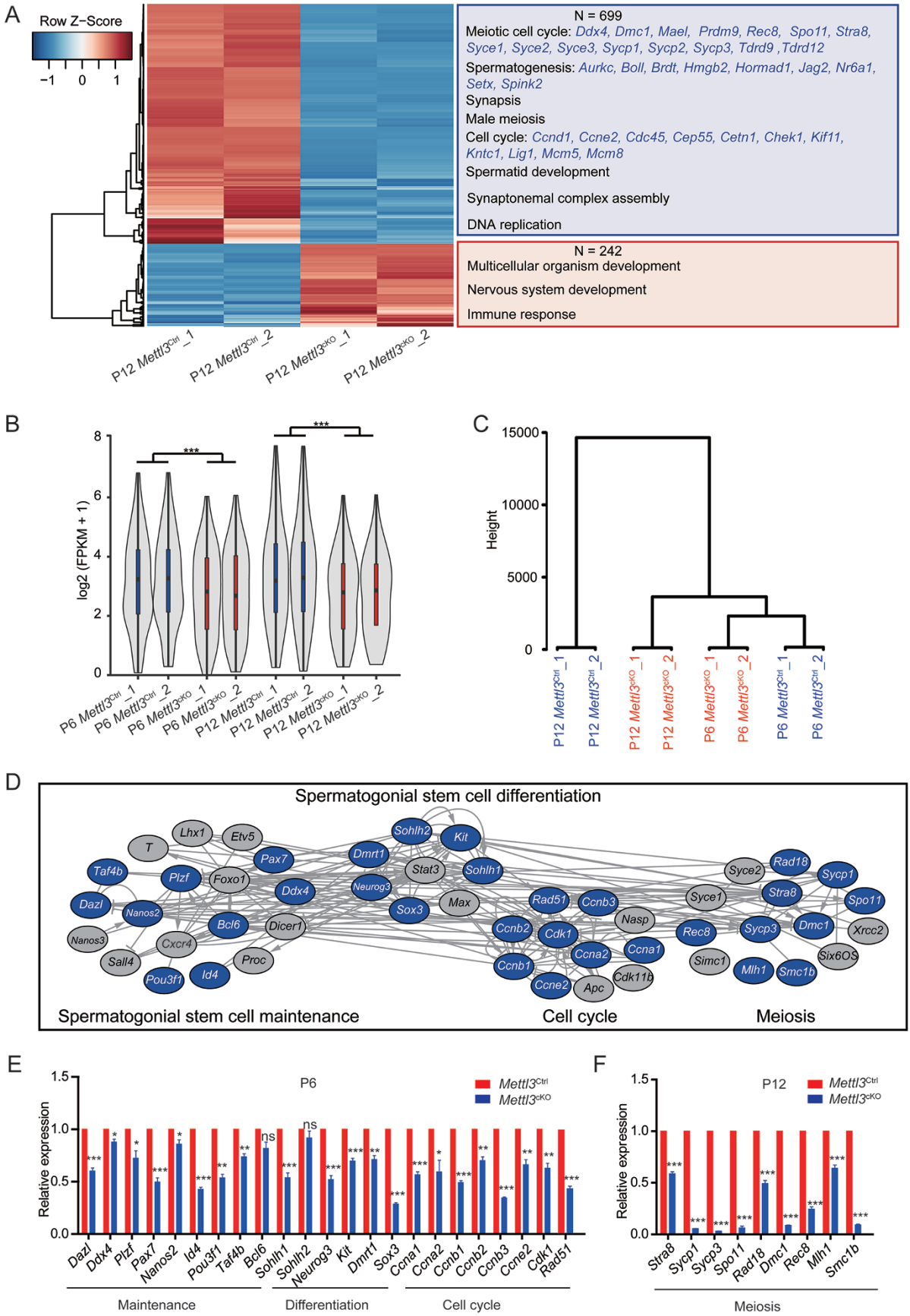
A
Row Z-Score
−1 0 1
N = 699
Meiotic cell cycle: Ddx4, Dmc1, Mael, Prdm9, Rec8, Spo11, Stra8, Syce1, Syce2, Syce3, Sycp1, Sycp2, Sycp3, Tdrd9 ,Tdrd12
Spermatogenesis: Aurkc, Boll, Brdt, Hmgb2, Hormad1, Jag2, Nr6a1, Setx, Spink2
Synapsis
Male meiosis
Cell cycle: Ccnd1, Ccne2, Cdc45, Cep55, Cetn1, Chek1, Kif11, Kntc1, Lig1, Mcm5, Mcm8
Spermatid development
Synaptonemal complex assembly
DNA replication
N = 242
Multicellular organism development
Nervous system development
Immune response
P12 Mettl3Ctrl_1
P12 Mettl3Ctrl_2
P12 Mettl3cKO_1
P12 Mettl3cKO_2
B
log2 (FPKM + 1)
***
P6 Mettl3Ctrl_1
P6 Mettl3Ctrl_2
P6 Mettl3cKO_1
P6 Mettl3cKO_2
P12 Mettl3Ctrl_1
P12 Mettl3Ctrl_2
P12 Mettl3cKO_1
P12 Mettl3cKO_2
C
Height
P12 Mettl3Ctrl_1
P12 Mettl3Ctrl_2
P12 Mettl3cKO_1
P12 Mettl3cKO_2
P6 Mettl3cKO_1
P6 Mettl3cKO_2
P6 Mettl3Ctrl_1
P6 Mettl3Ctrl_2
D
Spermatogonial stem cell differentiation
Spermatogonial stem cell maintenance
Cell cycle
Meiosis
E
P6
Mettl3Ctrl
Mettl3cKO
Relative expression
Maintenance
Differentiation
Cell cycle
F
P12
Meiosis

mammalian tissues has remained elusive due to the early lethality of *Mettl3*-deficient mice [24]. Here, we presented a number of findings demonstrating the significance of m^{6}A in male fertility and spermatogenesis: (1) conditional deletion of *Mettl3* in germ cells led to defective spermatogonial differentiation and meiosis, demonstrating an essential role of METTL3-mediated m^{6}A modification in male fertility and spermatogenesis (Figures 1 and 2). (2) Transcriptome analysis and qRT-PCR assays revealed that deletion of *Mettl3* resulted in downregulation of several spermatogenesis-related genes (Figure 3). (3) The *Mettl3* deficiency dysregulated alternative splicing of spermatogenesis-related genes (Figure 4). Thus, our study provides evidence that m^{6}A plays a significant role in regulating spermatogenesis by affecting the expression and splicing of spermatogenesis-related genes.

Previous studies have shown that deletion of *Alkbh5*, one of the m^{6}A demethylases, led to impaired fertility with compromised production of meiotic metaphase-stage spermatocytes [8], suggesting a regulatory role of m^{6}A in spermatogenesis. However, the underlying mechanism remains unknown. Compared to the phenotypes of *Alkbh5* knockout mice, the defects in *Mettl3*^{cKO} mice arise much earlier and are more severe, suggesting a less redundant and moreover, indispensable function of METTL3-catalyzed m^{6}A formation in tissue development. The essential role of both the m^{6}A demethylase and methyltransferase in spermatogenesis also suggest that the overall balance of RNA m^{6}A modification is key to maintain the differentiation program during spermatogenesis. Highly dynamic developmental processes, such as the spermatogenesis, require dynamic gene expression involving multiple layers of transcriptional regulation. Hence both demethylase- and methyltransferase-catalyzed m^{6}A modifications play an important role in normal development.

Spermatogenesis is a complicated process involving dynamic spermatogonial differentiation coupled with meiosis. DNA methylation and demethylation, histone modification, together with lncRNAs, microRNAs, piRNA and many transcriptional factors have been shown to participate in regulating spermatogenic progression by modulating gene expression [42-48]. Alternative splicing is another important mechanism to regulate gene expression, and a recent report showed that *Bcas2*, an important alternative splicing factor, functions in spermatogonia and is involved in the transition to meiosis through regulating alternative mRNA splicing [49].

Recent studies have implicated an essential regulatory role of m^{6}A in mRNA splicing [4, 11, 16, 19, 24, 26, 27, 50-54]. First, m^{6}A alters the local structure in mRNA to facilitate the binding of some HNRNP proteins [51, 53]. Alarcon *et al*. [16] revealed that modulation of METTL3 and HNRNPA2B1 causes similar changes to alternative splicing; Second, the m^{6}A reader YTHDC1 promotes SRSF3 but antagonizes SRSF10 binding to mRNAs and affects mRNA splicing [11]. An m^{6}A-modified *Sxl* intron regulates the adjacent exon splicing and controls *Drosophila* sex determination [26, 27, 52]. Moreover, Ye *et al*. [54] demonstrated an essential role of m^{6}A in regulating replication transcription activator pre-mRNA splicing in Kaposi's sarcoma-associated herpesvirus.

Nevertheless, the recent study of Ke *et al*. [55] showed that only 99 exons from ~2 000 alternatively spliced cassette exons containing m^{6}A have a significantly changed inclusion level upon Mettl3 depletion using Quantas software with FDR < 5% and ΔPSI $\geq$ 0.1, raising a question regarding the role of m^{6}A in the regulation of alternative splicing. However, many factors may affect the callings of alternative splicing, such as sequencing depth, the analysis pipeline and parameters [56-58]. We further analyzed the RNA-seq datasets [19, 24, 50, 51] used in the Ke *et al*. study [55] to detect the changed alternative splicing events by rMATS [34], a popular software used in alternative splicing analysis with FDR < 0.05. The number of changed alternative splicing events

Figure 3 *Mettl3* deletion alters expression pattern of genes involved in mouse spermatogenesis. **(A)** Heatmap showing the differentially expressed genes between *Mettl3*^{Ctrl} and *Mettl3*^{cKO} testes at P12 and their function enrichment. Two-fold expression difference and *P* = 0.05 as the cutoff. The enriched Gene Ontology (GO) terms of the biological process category in down or upregulated genes in *Mettl3*^{cKO} samples were shown on the right panels. **(B)** Violin plot of expression levels of germ cell specifically expressed genes in *Mettl3*^{Ctrl} and *Mettl3*^{cKO} samples at P6 and P12. The log2-transformed expression level (FPKM) was used for drawing the plot. *** means the *P* < 10e-5, as calculated by the Wilcoxon signed-rank paired test. **(C)** The unsupervised hierarchical cluster analysis for the expression of germ cell specifically expressed genes in *Mettl3*^{Ctrl} and *Mettl3*^{cKO} samples at P6 and P12. **(D)** The interaction network showing genes involved in spermatogenesis regulation. The downregulated genes in *Mettl3*^{cKO} testes which had been validated by qRT-PCR marked in blue. The regulation relationships were produced by pathway studio; the positive, negative regulation among these genes was marked as arrow, T-head respectively, while the regulation with unknown effects between two genes were connected directly. **(E**, **F)** qRT-PCR validation of downregulated genes involved in spermatogenesis in *Mettl3*^{cKO} testes at P6 **(E)** and P12 **(F)**. Student's *t*-test was performed and data was shown as mean ± SEM. of three independent experiments. **P* < 0.05, ***P* < 0.01, ****P* < 0.001; ns, no significance.

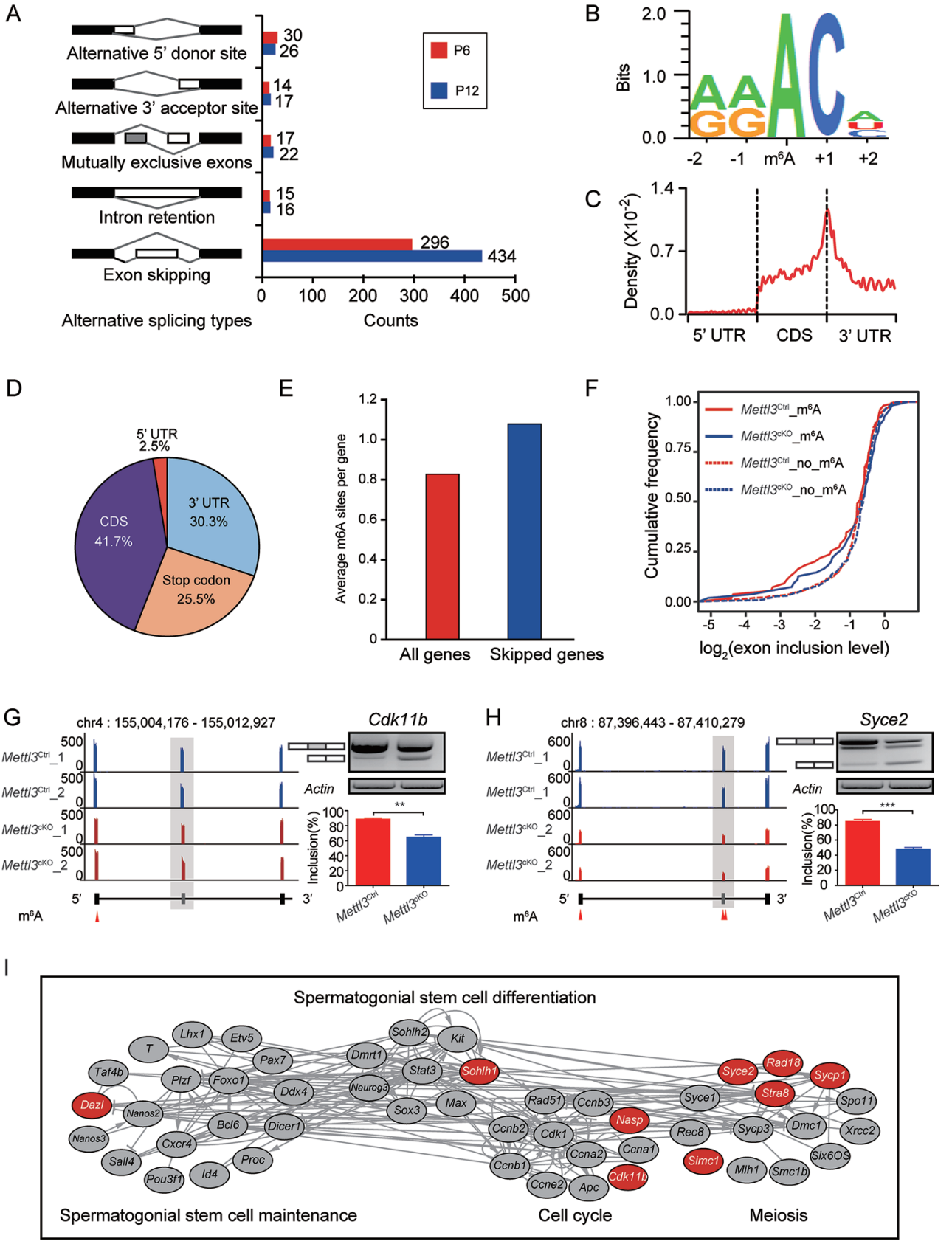
A
Alternative 5' donor site
Alternative 3' acceptor site
Mutually exclusive exons
Intron retention
Exon skipping
30
26
14
17
17
22
15
16
296
434
P6
P12
0
100
200
300
400
500
Counts
Alternative splicing types
B
Bits
2.0
1.0
0.0
-2
-1
m6A
+1
+2
C
Density (X10-2)
1.4
0.7
0.0
5' UTR
CDS
3' UTR
D
5' UTR 2.5%
3' UTR 30.3%
CDS 41.7%
Stop codon 25.5%
E
Average m6A sites per gene
1.2
1.0
0.8
0.6
0.4
0.2
0
All genes
Skipped genes
F
Cumulative frequency
1.00
0.75
0.50
0.25
0.00
Mettl3Ctrl_m6A
Mettl3cKO_m6A
Mettl3Ctrl_no_m6A
Mettl3cKO_no_m6A
-5
-4
-3
-2
-1
0
log2(exon inclusion level)
G
chr4 : 155,004,176 - 155,012,927
Cdk11b
Mettl3Ctrl_1
Mettl3Ctrl_2
Mettl3cKO_1
Mettl3cKO_2
500
0
Actin
Inclusion(%)
100
80
60
40
20
0
**
5'
3'
m6A
Mettl3Ctrl
Mettl3cKO
H
chr8 : 87,396,443 - 87,410,279
Syce2
600
***
I
Spermatogonial stem cell differentiation
Lhx1
Etv5
T
Pax7
Taf4b
Plzf
Foxo1
Dazl
Nanos2
Nanos3
Bcl6
Cxcr4
Sall4
Pou3f1
Id4
Proc
Ddx4
Dicer1
Dmrt1
Sohlh2
Kit
Stat3
Sohlh1
Neurog3
Sox3
Max
Rad51
Ccnb3
Nasp
Ccnb2
Cdk1
Ccna2
Ccna1
Ccnb1
Ccne2
Apc
Cdk11b
Syce2
Rad18
Sycp1
Syce1
Stra8
Spo11
Rec8
Sycp3
Dmc1
Xrcc2
Simc1
Mlh1
Smc1b
Six6OS
Spermatogonial stem cell maintenance
Cell cycle
Meiosis

varied from dozens to thousands in different tissues or cell types, indicating that m^{6}A regulates alternative splicing events in a tissue-dependent manner (Supplementary information, Figure S4R). Given that one mRNA can be expressed by alternative splicing according to different regulatory programs, mild alternative splicing events can be sufficient to induce important functional changes [19, 59]. Future systematic analysis of m^{6}A single-site resolution of pre-mRNAs will be able to give straight forward answers how m^{6}A regulates mRNA splicing.

Our findings demonstrated an additional mechanism for METTL3 in spermatogenesis by regulating the alternative splicing of mRNAs. We found that many important spermatogenesis-regulating genes, such as *Sohlh1* and *Dazl* [35-37, 49], carried m^{6}A modification and exhibited altered splicing pattern in *Mettl3*^{cKO} mice. This indicates that the loss of m^{6}A modification on these genes upon *Mettl3* deletion indeed influenced their alternative splicing pattern and resulted in defective spermatogenesis.

Mettl3-mediated m^{6}A modification was a prerequisite for the initiation of spermatogenesis from undifferentiated spermatogonia since both the initial spermatogonial differentiation and the initial meiosis were severely blocked upon *Mettl3* disruption, as evidenced by the findings that KIT-positive cells were significantly reduced and spermatocytes could not reach the pachytene stage of meiotic prophase in *Mettl3*^{cKO} testes. Thus, our findings provide strong evidence for deciphering the *in vivo* functions of METTL3-mediated m^{6}A modification in mouse spermatogenesis.

Materials and Methods

Mouse

The mice used in this study were B6D2F1 (C57BL/6 × DBA2), DBA2 and C57BL6 strains. Specific pathogen-free-grade mice were purchased from Beijing Vital River laboratory animal center and housed in the animal facilities of the Institute of Zoology, Chinese Academy of Sciences. All animal experiments were carried out in accordance with the guidelines for the Use of Animals in Research issued by the Institute of Zoology, Chinese Academy of Sciences.

Mouse breeding

Mettl3$^{flox/+}$ mice were generated by the CRISPR-Cas9 system-assisted homologous recombination. *Vasa-Cre* transgenic mice were a gift from professor Jia-Hao Sha, Nanjing Medical University. *Mettl3*$^{flox/+}$*Vasa-Cre* mice were obtained by mating *Mettl3*$^{flox/+}$ and *Vasa-Cre* mice and *Mettl3*$^{flox/flox}$ mice were obtained by mating *Mettl3*$^{flox/+}$ and *Mettl3*$^{flox/+}$ mice. *Mettl3*$^{flox/+}$*Vasa-Cre* and *Mettl3*$^{flox/flox}$ were mated to generate *Mettl3*$^{flox/-}$*Vasa-Cre* mice (*Mettl3*^{cKO}).

Construction of gene targeting vector

The T7-Cas9 vector was from our lab. The T7-sgRNA vector was digested with BsaI enzyme (NEB) and the linearized vector was gel purified. A pair of oligonucleotides for each targeting site (*Mettl3* intron 1 and intron 4) was annealed and ligated to linearized vector. All oligonucleotides were listed in the Supplementary information, Table S1.

In vitro preparation of sgRNAs, Cas9 mRNA and oligonucleotide DNAs for microinjection

All RNAs prepared for microinjection were *in vitro* transcribed. SgRNAs and Cas9 mRNA were transcribed by the HiScribe T7 *In Vitro* Transcription Kit (NEB). The Cas9 mRNA was capped with the m7G (5′) ppp (5′) G RNA Cap Structure Analog (NEB) by T7 transcriptase. All RNAs were dissolved in DEPC water and stored in −80 °C.

Oligonucleotides used for CRISPR-Cas9 system-assisted homologous recombination through embryo injection were synthetized in Integrated DNA Technologies. All oligonucleotides were listed in the Supplementary information, Table S1.

Intracytoplasmic RNA microinjection

The intracytoplasmic RNA microinjection was performed according to a previous report. Briefly, one-cell-stage embryos were collected at 0.5 day post coitum (dpc). Each embryo was microinjected with 25 ng/μl L-sgRNA, 25 ng/μl R-sgRNA, 100 ng/μl

Figure 4 *Mettl3*-mediated m^{6}A regulates alternative splicing of genes involved in spermatogenesis. **(A)** Schematics and statistics of the five types of alternative splicing events in *Mettl3*^{Ctrl} and *Mettl3*^{cKO} testes at P6 and P12. The differential alternative splicing events were identified by rMATS and the FDR = 0.05 were used as cutoff. Each group sample included two replicates. **(B)** The logo plot for bases adjacent to m^{6}A sites. All 12 516 putative m^{6}A residues were used to enrich the m^{6}A motif and the plot was produced by WebLogo. **(C)** Distribution of m^{6}A sites across the length of mRNA transcripts. **(D)** Transcriptome-wide distribution of m^{6}A sites. Pie charts showing the percentage of m^{6}A sites in distinct RNA sequence types: 5' UTR, CDS, Stop codon and 3' UTR. **(E)** The average m^{6}A site frequency per gene in all genes and in differentially spliced genes in *Mettl3*^{Ctrl} testes at P12. **(F)** The cumulative frequency curve for the alternative exon inclusion ratio in *Mettl3*^{Ctrl} and *Mettl3*^{cKO} testes at P12. The exon inclusion level was calculated by alternative exon coverage divided by constitutive exon coverage and transformed by log2. The exons containing m^{6}A sites in *Mettl3*^{cKO} testes showed lower coverage level than in *Mettl3*^{Ctrl} testes ($P < 0.01$, Wilcoxon signed-rank paired test). No significant difference was exhibited between exons without m^{6}A modification. **(G**, **H)** Distribution of RNA-seq reads of *Cdk11b* **(G)** and *Syce2* **(H)** in *Mettl3*^{Ctrl} and *Mettl3*^{cKO} testes samples, the alternative exon of each gene was marked in grey and shadow. The m^{6}A site location was marked as a red triangle. The exon skipping event was validated by RT-PCR (right panel). **(I)** The interaction network showing genes involved in spermatogenesis regulation. The genes containing alternative exons which had been validated by RT-PCR were marked in red. The regulation relationships were produced by Pathway Studio; the positive, negative regulation among these genes was marked as arrow, T-head respectively, while the regulation with unknown effects between two genes was connected directly.

Cas9 mRNA, 50 ng/μl L-loxp oligonucleotide and 50 ng/μl R-loxp oligonucleotide into the cytoplasm. After microinjection, surviving embryos were implanted on the same day into the oviduct of pseudopregnant B6D2F1 female mice. Full-term pups were obtained by natural labor at 19.5 dpc.

Immunohistochemical analysis

For immunostaining analysis: testes were fixed in 4% paraformaldehyde overnight at 4 °C. Following dehydration, the samples were embedded in paraffin and sectioned (5 μm). After dewaxing and hydration, the sections were boiled in an antigen retrieval buffer (0.01 M citric acid/sodium citrate, pH 6.0) for 10 min using a microwave oven, washed in PBS three times and permeated in 0.2% Triton X-100 for 15 min. The sections were blocked with 5% BSA in PBS for 2 h at room temperature before adding primary antibodies. The samples were washed three times in PBS after incubating at 4 °C overnight and then incubated with secondary antibodies for 2 h at room temperature. After washing in PBS three times, the sections were incubated in 2 μg/ml of DAPI (Molecular Probes, D1306) for 10 min at room temperature and washed in PBS three times. Sections were mounted on slices with Dako Fluorescence Mounting Medium (Dako Canada, ON, Canada). The immunohistochemical analysis of STRA8 were imaged with a Leica Aperio VERSA 8 microscope (Leica Biosystems, Germany). The immunofluorescence staining was imaged with a laser scanning confocal microscope LSM780 (Carl Zeiss, Germany). All the antibodies were listed in the Supplementary information, Table S2.

Genotyping of mice

First, all mice were genotyped with the tail DNA. Two pair of primers were used to detect the loxp insertion into the *Mettl3* intron 1 (L-loxp-forward and L-loxp-reverse) and intron 4 (R-loxp-forward and R-loxp-reverse). The product sizes were 222 bp and 335 bp with the loxp sequence insertion into *Mettl3* intron 1 and intron 4, respectively; whereas the product sizes from WT were 182 bp and 295 bp, respectively. Cre recombinase was detected by the *Vasa-Cre* primers and the product of PCR was 240 bp. The PCR reaction conditions were as follows: 95 °C, 2 min; 95 °C, 30 s, 61 °C, 30 s, 72 °C, 30 s, 35 cycles; 72 °C, 5 min. Then the germ cells were used to confirm the deletion of *Mettl3* with the primers of L-loxp-forward and R-loxp-reverse and the product of *Mettl3* deletion was 318 bp whereas the WT product was 2 554 bp. The PCR reaction conditions were as follows: 95 °C, 5 min; 95 °C, 30 s, 61 °C, 30 s, 72 °C, 2.5 min, 35 cycles; 72 °C, 10 min. All primers are listed in the Supplementary information, Table S3.

Histological analysis

For histological analysis: testes from *Mettl3*^{Ctrl} and *Mettl3*^{cKO} male mouse were fixed in Modified Davidson's Fluid (Formaldehyde:Glacial acetic acid:Ethanol:H_2O = 6:3:1:10) overnight at room temperature. The testes were dehydrated stepwise through an ethanol series (70%, 80%, 90%, 100% ethanol) and processed for paraffin embedding. 5 μm sections were cut with a Leica slicing machine (Leica RM2235, Leica Biosystems, Germany) and mounted on poly-D-lysine coated glass slices (Zhong Shan Golding Bridge biotechnology, Beijing, China). After dewaxing and hydration, the sections were stained with H&E using standard methods and imaged with a Leica Aperio VERSA 8 microscope (Leica Biosystems, Germany).

TUNEL analysis

The TUNEL assay was performed using the TUNEL BrightRed Apoptosis Detection Kit (Vazyme) according to the manufacturer's instructions. Briefly, sections were permeabilized by protein K and labeled with rTdT reaction mix for 1 h at 37 °C, reaction was stopped by 1× PBS. After washing in PBS, the sections were incubated in 2 μg/ml of DAPI (Molecular Probes, D1306) for 10 min at room temperature and washed in PBS. Sections were mounted on slices with Dako Fluorescence Mounting Medium (Dako Canada, ON, Canada). Images were obtained using a laser scanning confocal microscope LSM780 (Carl Zeiss).

RNA extraction and qRT-PCR

Total RNA was extracted with TRIzol reagent (Invitrogen, 15596-018) from whole testes. After removing the genomic DNA with the RNase-Free DNase I Kit (Promega, M6101), 1 μg total RNA reverse-transcribed into cDNAs using the reverse Transcription System (Promega, A3500). qRT-PCR was performed using a SYBR Premix Ex Taq kit (TaKaRa, RR420A) on Agilent Stratagene Mx3005P. Relative gene expression was analyzed based on the $2^{-\Delta\Delta Ct}$ method with *Actin* as internal control. At least three independent experiments were analyzed. All primers were listed in the Supplementary information, Table S3.

m^{6}A-miCLIP-seq

Single-base resolution high-throughput sequencing of the mouse testes methylome was carried out according to previously reported methods [60] with some modifications. Briefly, mRNA was purified using a Dynabeads® mRNA Purification Kit (Life Technologies, 61006) and fragmented into around 100 nt fragments using the RNA fragmentation reagent (Life Technologies, AM8740). 5 μg mRNA was incubated with 10 μg of anti-m^{6}A antibody (Abcam, ab151230) in 450 μl immunoprecipitation buffer (50 mM Tris, pH 7.4, 100 mM NaCl, 0.05% NP-40) and incubated at 4 °C for 2 h with gentle rotation. The mixture was transferred to a clear flat-bottom 96-well plate (Corning) on ice and irradiated three times with 0.15 J/cm^2 at 254 nm in a CL-1000 Ultraviolet Crosslinker (UVP). After irradiation, the mixture was collected together and then immunoprecipitated by incubation with dynabeads protein A (Life Technologies, 10008D) at 4 °C by rotating for another 2 h. After extensive washing, end-repair and linker ligation was performed on-bead. Finally, the bound RNA fragments were eluted from the beads with 2 μg/μl proteinase K in PK buffer (100 mM Tris-HCl, pH 7.4, 50 mM NaCl, 10 mM EDTA) by digestion at 55 °C for 20 min. RNA was isolated from the eluate by phenol-chloroform (Life Technologies, AM9730) extraction and ethanol precipitation. Purified RNA was reverse transcribed with Superscript III reverse transcriptase (Life Technologies, 18080093) according to the manufacturer's protocol as described previously [18, 61]. cDNA was size-selected on a 6% TBE-Urea gel (Life Technologies, EC68655BOX) and regions corresponding to 70-100 nt were used for further analysis. Thus, purified cDNA was circularized with Circligase II (Epicentre, CL9021K) and re-linearized with BamHI (NEB, R0136M). Libraries were PCR amplified with Accuprime Supermix 1 enzyme for 18 cycles and size-selected on an 8% TBE gel (Life Technologies, EC62155BOX). Sequencing was carried out on an Illumina HiSeq 3000 platform according to the manufacturer's instructions.

m^{6}A-RIP-qPCR

The procedure of m^{6}A immunoprecipitation (m^{6}A-RIP) was modified from previously reported methods [23]. In brief, purified mRNAs from P6/P12 mouse testes were digested by DNase I and then fragmented into ~300 nt fragments by 30 s incubation at 94 °C in RNA fragmentation reagent (Life technologies, AM8740). This reaction was then stopped with stop solution (Life technologies, AM8740), followed by standard ethanol precipitation and collection. 12 μg anti-m^{6}A polyclonal antibody (Synaptic Systems) was pre-incubated with 50 μl Dynabeads Protein A (Life technologies, 10013D) in IPP buffer (150 mM NaCl, 0.1% NP-40, 10 mM Tris-HCl, pH 7.4) for 1 h at room temperature. After pre-heating at 75 °C for 5 min and chilling on ice immediately, 6 μg mRNAs were added to the above prepared antibody-beads mixture and incubated for 4 h at 4 °C by rotating. After extensive washing, bound RNAs were extracted by proteinase K digestion, phenol-chloroform (Life Technologies, AM9730) extraction and ethanol precipitation. The enrichment of m^{6}A was quantified through qPCR as reported [23]. m^{6}A-RIP-qPCR primers are listed in the Supplementary information, Table S3.

RNA-seq library preparation and data processing

Total RNA was extracted from cultured cells by TRIzol reagent (Invitrogen, 15596-018). For RNA-seq library construction, the PolyA+ tailed RNA purification was performed for each sample using a Dynabeads mRNA purification kit (Ambion, 61006). The cDNA library was generated with a KAPA Stranded mRNA-Seq Kit (KAPA, KR0960) protocol. Sequencing was performed on an Illumina HiSeq 3000 platform with 101 bp paired-end-sequencing reactions. The RNA-seq reads of each sample were mapped to the mouse mm9 genome assembly independently by the HISAT2 software using the annotated gene structures as templates. Default parameters of HISAT2 were used except with the options "--dta-cufflinks" and "--rna-strandness RF" opening [62]. Reads with unique genome location were retained for gene expression calculation using Cufflinks (version 2.0.2) with the option "--GTF" [63]. Genes with no less than 0.5 FPKM in at least one sample were used for the differentially expressed genes analysis.

Alternative splicing analysis

Reads with a unique genome location in SAM format were used for the splicing events identification. The AS events between the two sample groups were identified using rMATS version 3.2.5 [34]. Five types of AS events from RNA-seq data with two replicates were identified. In each rMATS run, the first group was compared to the second group to identify differentially spliced events with FDR less than 0.05. The alternative exon accumulation levels in each sample were calculated using methods previously described. RT-PCR validation of alternative splicing events were performed with cDNA reverse-transcribed from mouse testes RNA. *Actin* was used as an internal control. All primers are listed in the Supplementary information, Table S3.

Analysis of miCLIP-sequencing data

The method of pre-processing for reads was performed essentially as previously reported [64]. The adaptor was trimmed by fastx_clipper fastx_toolkit (http://hannonlab.cshl.edu/fastx_toolkit/). Low quality bases were filtered by fastq_filter.pl, a custom perl script from CLIP Tool Kit (CTK) [65] and reads shorter than 24 nt discarded. After trimming, reads without a barcode marker sequence or within large fragment (length > 60 nt) are discarded to eliminate unspecific RNA tags. Based on the same criteria of a previously reported approach to process paired-end data, the forward reads were demultiplexed based on 5′ barcodes for individual replicates by fastq2collapse to remove PCR amplified reads and the reverse reads were reverse-complemented and processed like their forward mates. Finally, the random barcodes of remaining reads were stripped by stripBarcode.pl and moved to read headers for downstream processing by the CIMS pipeline.

Remaining reads were mapped to the mouse genome (version mm9) with BWA (v0.7.10) [66] and allowed ≤ 0.06 error rate (substitutions, insertions or deletions) per read as online CTK Documentation (https://zhanglab.c2b2.columbia.edu/index.php/CTK_Documentation). To identify the m^{6}A locus, the mode of mutation calling was performed as previously reported with minor modification [60]. For each mutation position, the coverage of a unique tag (k) and mutations (m) was determined by the CIMS.pl program [67]. The positions within $k \geq 15$ and $m/k \leq 50\%$ were kept and only mutation positions within the RRACH motif were identified as m^{6}A for downstream analysis to exclude the potential m^{6}Am modification [60]. The logo plot for bases adjacent to m^{6}A was generated with WebLogo [68].

Other tools

The unsupervised hierarchical cluster analysis performed by the hcluster function of the amap package in R. Point plots were produced by the smoothScatter functions of R. And the Pearson correlation coefficients shown in the figures. The heatmap was produced by the heatmap.2 function of R. Gene ontology analysis of differentially expressed genes was analyzed in DAVID [69, 70] and biological processes were selected based on *P*-values smaller than 0.05 and the figures were produced by ggplot2. The interaction relationship of spermatogenesis related genes was constructed by Pathway Studio [71] based on the regulation reported in public reference and the network was showed by the Cytoscape [72]. The cumulative frequency curve and violin plot were also produced by ggplot2. The RNA-seq reads distribution were exhibited in IGV browser [73].

Quantification and statistical analysis

Statistical parameters including statistical analysis, statistical significance and n value are reported in the Figure legends. Statistical analyses were performed using Prism Software (GraphPad). For statistical comparison, Student's t-test was employed. A value of $P < 0.05$ was considered significant.

Data and software availability

The accession number for the sequencing data reported in this paper is NCBI GEO: GSE99773. This parent directory includes the following datasets: GEO: GSE99771 (RNA-seq) and GEO: GSE99772 (m^{6}A-miCLIP-seq). The public RNA-seq datasets (GSE53249, GSE56010, GSE61997 and GSE37005) for alternative splicing events identification by rMATS were downloaded from GEO database.

Acknowledgments

We thank Dr Y-L Zhao from Beijing Institute of Genomics,

Chinese Academy of Sciences for scientific suggestion. This work was supported by the National Natural Science Foundation of China (31422038, 31471395, 31625016 and 31670824), the National Basic Research Program of China (2014CB964800, 2016YFC0900300), CAS Strategic Priority Research Program (XDB14030300, QYZDY-SSW-SMC027/002, QYZDB-SSW-SMC022). We thank BIG sequencing core facility for sequencing.

Authors Contributions

WL, Y-GY and QZ conceived this project and supervised all the experiments and data analysis. Y-GY, WL, QZ, KX, G-HF, YY and B-FS analyzed the data and wrote the manuscript. YY performed m^{6}A-miCLIP and m^{6}A-RIP-qPCR assays. G-HF performed bioinformatics analysis with assistance from B-FS, Y-SC and X-JW. KX performed molecular biology, protein chemistry, cell culture and mouse experiments with assistance from J-QC, Y-FL, X-XZ, C-XW, L-YJ, CL, Z-YZ.

Competing Financial Interests

The authors declare no competing financial interests.

References

1 Zhao BS, Roundtree IA, He C. Post-transcriptional gene regulation by mRNA modifications. *Nat Rev Genet* 2017; **18**:31-42.
2 Bokar JA, Shambaugh ME, Polayes D, Matera AG, Rottman FM. Purification and cDNA cloning of the AdoMet-binding subunit of the human mRNA (N^6-adenosine)-methyltransferase. *RNA* 1997; **3**:1233-1247.
3 Liu J, Yue Y, Han D, *et al.* A METTL3-METTL14 complex mediates mammalian nuclear RNA N^6-adenosine methylation. *Nat Chem Biol* 2014; **10**:93-95.
4 Ping XL, Sun BF, Wang L, *et al.* Mammalian WTAP is a regulatory subunit of the RNA N^6-methyladenosine methyltransferase. *Cell Res* 2014; **24**:177-189.
5 Schwartz S, Mumbach MR, Jovanovic M, *et al.* Perturbation of m^{6}A writers reveals two distinct classes of mRNA methylation at internal and 5' sites. *Cell Rep* 2014; **8**:284-296.
6 Wang Y, Li Y, Toth JI, Petroski MD, Zhang Z, Zhao JC. N^6-methyladenosine modification destabilizes developmental regulators in embryonic stem cells. *Nat Cell Biol* 2014; **16**:191-198.
7 Jia G, Fu Y, Zhao X, *et al.* N^6-methyladenosine in nuclear RNA is a major substrate of the obesity-associated FTO. *Nat Chem Biol* 2011; **7**:885-887.
8 Zheng G, Dahl JA, Niu Y, *et al.* ALKBH5 is a mammalian RNA demethylase that impacts RNA metabolism and mouse fertility. *Mol Cell* 2013; **49**:18-29.
9 Wang X, Lu Z, Gomez A, *et al.* N^6-methyladenosine-dependent regulation of messenger RNA stability. *Nature* 2014; **505**:117-120.
10 Wang X, Zhao BS, Roundtree IA, *et al.* N^6-methyladenosine modulates messenger RNA translation efficiency. *Cell* 2015; **161**:1388-1399.
11 Xiao W, Adhikari S, Dahal U, *et al.* Nuclear m^{6}A reader YTHDC1 regulates mRNA splicing. *Mol Cell* 2016; **61**:507-519.
12 Li A, Chen YS, Ping XL, *et al.* Cytoplasmic m^{6}A reader YTHDF3 promotes mRNA translation. *Cell Res* 2017; **27**:444-447.
13 Shi H, Wang X, Lu Z, *et al.* YTHDF3 facilitates translation and decay of N^6-methyladenosine-modified RNA. *Cell Res* 2017; **27**:315-328.
14 Meyer KD, Patil DP, Zhou J, *et al.* 5' UTR m^{6}A promotes cap-independent translation. *Cell* 2015; **163**:999-1010.
15 Zhou J, Wan J, Gao X, Zhang X, Jaffrey SR, Qian SB. Dynamic m^{6}A mRNA methylation directs translational control of heat shock response. *Nature* 2015; **526**:591-594.
16 Alarcon CR, Goodarzi H, Lee H, Liu X, Tavazoie S, Tavazoie SF. HNRNPA2B1 is a mediator of m^{6}A-dependent nuclear RNA processing events. *Cell* 2015; **162**:1299-1308.
17 Alarcon CR, Lee H, Goodarzi H, Halberg N, Tavazoie SF. N^6-methyladenosine marks primary microRNAs for processing. *Nature* 2015; **519**:482-485.
18 Patil DP, Chen CK, Pickering BF, *et al.* m^{6}A RNA methylation promotes XIST-mediated transcriptional repression. *Nature* 2016; **537**:369-373.
19 Zhao X, Yang Y, Sun BF, *et al.* FTO-dependent demethylation of N^6-methyladenosine regulates mRNA splicing and is required for adipogenesis. *Cell Res* 2014; **24**:1403-1419.
20 Fustin JM, Doi M, Yamaguchi Y, *et al.* RNA-methylation-dependent RNA processing controls the speed of the circadian clock. *Cell* 2013; **155**:793-806.
21 Xiang Y, Laurent B, Hsu CH, *et al.* RNA m^{6}A methylation regulates the ultraviolet-induced DNA damage response. *Nature* 2017; **543**:573-576.
22 Aguilo F, Zhang F, Sancho A, *et al.* Coordination of m^{6}A mRNA methylation and gene transcription by ZFP217 regulates pluripotency and reprogramming. *Cell Stem Cell* 2015; **17**:689-704.
23 Chen T, Hao YJ, Zhang Y, *et al.* m^{6}A RNA methylation is regulated by microRNAs and promotes reprogramming to pluripotency. *Cell Stem Cell* 2015; **16**:289-301.
24 Geula S, Moshitch-Moshkovitz S, Dominissini D, *et al.* Stem cells. m^{6}A mRNA methylation facilitates resolution of naive pluripotency toward differentiation. *Science* 2015; **347**:1002-1006.
25 Zhao BS, Wang X, Beadell AV, *et al.* m^{6}A-dependent maternal mRNA clearance facilitates zebrafish maternal-to-zygotic transition. *Nature* 2017; **542**:475-478.
26 Haussmann IU, Bodi Z, Sanchez-Moran E, *et al.* m^{6}A potentiates *Sxl* alternative pre-mRNA splicing for robust *Drosophila* sex determination. *Nature* 2016; **540**:301-304.
27 Lence T, Akhtar J, Bayer M, *et al.* m^{6}A modulates neuronal functions and sex determination in *Drosophila*. *Nature* 2016; **540**:242-247.
28 Shen L, Liang Z, Gu X, *et al.* N^6-methyladenosine RNA modification regulates shoot stem cell fate in *Arabidopsis*. *Dev Cell* 2016; **38**:186-200.
29 Gallardo T, Shirley L, John GB, Castrillon DH. Generation of a germ cell-specific mouse transgenic Cre line, *Vasa-Cre*. *Genesis* 2007; **45**:413-417.
30 Li L, Dong J, Yan L, *et al.* Single-cell RNA-seq analysis maps development of human germline cells and gonadal niche interactions. *Cell Stem Cell* 2017; **20**:891-892.
31 Handel MA, Schimenti JC. Genetics of mammalian meiosis: regulation, dynamics and impact on fertility. *Nat Rev Genet* 2010; **11**:124-136.

32 Song HW, Wilkinson MF. Transcriptional control of spermatogonial maintenance and differentiation. *Semin Cell Dev Biol* 2014; **30**:14-26.
33 Chen SR, Liu YX. Regulation of spermatogonial stem cell self-renewal and spermatocyte meiosis by sertoli cell signaling. *Reproduction* 2015; **149**:R159-R167.
34 Shen S, Park JW, Lu ZX, *et al.* rMATS: robust and flexible detection of differential alternative splicing from replicate RNA-Seq data. *Proc Natl Acad Sci USA* 2014; **111**:E5593-E5601.
35 Ballow D, Meistrich ML, Matzuk M, Rajkovic A. *Sohlh1* is essential for spermatogonial differentiation. *Dev Biol* 2006; **294**:161-167.
36 Barrios F, Filipponi D, Campolo F, *et al*. SOHLH1 and SOHLH2 control Kit expression during postnatal male germ cell development. *J Cell Sci* 2012; **125**:1455-1464.
37 Suzuki H, Ahn HW, Chu T, *et al*. SOHLH1 and SOHLH2 coordinate spermatogonial differentiation. *Dev Biol* 2012; **361**:301-312.
38 Alekseev OM, Bencic DC, Richardson RT, Widgren EE, O'Rand MG. Overexpression of the Linker histone-binding protein tNASP affects progression through the cell cycle. *J Biol Chem* 2003; **278**:8846-8852.
39 Li T, Inoue A, Lahti JM, Kidd VJ. Failure to proliferate and mitotic arrest of CDK11(p110/p58)-null mutant mice at the blastocyst stage of embryonic cell development. *Mol Cell Biol* 2004; **24**:3188-3197.
40 Richardson RT, Alekseev O, Alekseev OM, O'Rand MG. Characterization of the NASP promoter in 3T3 fibroblasts and mouse spermatogenic cells. *Gene* 2006; **371**:52-58.
41 Richardson RT, Alekseev OM, Grossman G, *et al.* Nuclear autoantigenic sperm protein (NASP), a linker histone chaperone that is required for cell proliferation. *J Biol Chem* 2006; **281**:21526-21534.
42 Bourc'his D, Bestor TH. Meiotic catastrophe and retrotransposon reactivation in male germ cells lacking Dnmt3L. *Nature* 2004; **431**:96-99.
43 Delaval K, Govin J, Cerqueira F, Rousseaux S, Khochbin S, Feil R. Differential histone modifications mark mouse imprinting control regions during spermatogenesis. *EMBO J* 2007; **26**:720-729.
44 Oakes CC, La Salle S, Smiraglia DJ, Robaire B, Trasler JM. Developmental acquisition of genome-wide DNA methylation occurs prior to meiosis in male germ cells. *Dev Biol* 2007; **307**:368-379.
45 Huszar JM, Payne CJ. MicroRNA 146 (*Mir146*) modulates spermatogonial differentiation by retinoic acid in mice. *Biol Reprod* 2013; **88**:15.
46 Goh WS, Falciatori I, Tam OH, *et al.* piRNA-directed cleavage of meiotic transcripts regulates spermatogenesis. *Genes Dev* 2015; **29**:1032-1044.
47 Akhade VS, Dighe SN, Kataruka S, Rao MR. Mechanism of Wnt signaling induced down regulation of mrhl long non-coding RNA in mouse spermatogonial cells. *Nucleic Acids Res* 2016; **44**:387-401.
48 Kataruka S, Akhade VS, Kayyar B, Rao MRS. Mrhl lncRNA mediates meiotic commitment of mouse spermatogonial cells by regulating Sox8 expression. *Mol Cell Biol* 2017; **37**:pii:e00632-16.
49 Liu W, Wang F, Xu Q, *et al.* BCAS2 is involved in alternative mRNA splicing in spermatogonia and the transition to meiosis. *Nat Commun* 2017; **8**:14182.
50 Dominissini D, Moshitch-Moshkovitz S, Schwartz S, *et al*. Topology of the human and mouse m^{6}A RNA methylomes revealed by m^{6}A-seq. *Nature* 2012; **485**:201-206.
51 Liu N, Dai Q, Zheng G, He C, Parisien M, Pan T. *N*^{6}-methyladenosine-dependent RNA structural switches regulate RNA-protein interactions. *Nature* 2015; **518**:560-564.
52 Kan L, Grozhik AV, Vedanayagam J, *et al*. The m^{6}A pathway facilitates sex determination in *Drosophila*. *Nat Commun* 2017; **8**:15737.
53 Liu N, Zhou KI, Parisien M, Dai Q, Diatchenko L, Pan T. *N*^{6}-methyladenosine alters RNA structure to regulate binding of a low-complexity protein. *Nucleic Acids Res* 2017; **10**:6051-6063
54 Ye F, Chen ER, Nilsen TW. Kaposi's sarcoma-associated herpesvirus utilizes and manipulates RNA *N*^{6}-adenosine methylation to promote lytic replication. *J Virol* 2017, doi:10.1128/JVI.00466-17.
55 Ke S, Pandya-Jones A, Saito Y, *et al*. m^{6}A mRNA modifications are deposited in nascent pre-mRNA and are not required for splicing but do specify cytoplasmic turnover. *Genes Dev* 2017; **31**:990-1006.
56 Stephan-Otto Attolini C, Pena V, Rossell D. Designing alternative splicing RNA-seq studies. Beyond generic guidelines. *Bioinformatics* 2015; **31**:3631-3637.
57 Pan Q, Shai O, Lee LJ, Frey BJ, Blencowe BJ. Deep surveying of alternative splicing complexity in the human transcriptome by high-throughput sequencing. *Nat Genet* 2008; **40**:1413-1415.
58 Zyprych-Walczak J, Szabelska A, Handschuh L, *et al*. The impact of normalization methods on RNA-Seq data analysis. *Biomed Res Int* 2015; **2015**:621690.
59 Merkestein M, Laber S, McMurray F, *et al*. FTO influences adipogenesis by regulating mitotic clonal expansion. *Nat Commun* 2015; **6**:6792.
60 Linder B, Grozhik AV, Olarerin-George AO, Meydan C, Mason CE, Jaffrey SR. Single-nucleotide-resolution mapping of m^{6}A and m^{6}Am throughout the transcriptome. *Nat Methods* 2015; **12**:767-772.
61 Konig J, Zarnack K, Rot G, *et al*. iCLIP reveals the function of hnRNP particles in splicing at individual nucleotide resolution. *Nat Struct Mol Biol* 2010; **17**:909-915.
62 Kim D, Langmead B, Salzberg SL. HISAT: a fast spliced aligner with low memory requirements. *Nat Methods* 2015; **12**:357-360.
63 Trapnell C, Williams BA, Pertea G, *et al*. Transcript assembly and quantification by RNA-Seq reveals unannotated transcripts and isoform switching during cell differentiation. *Nat Biotechnol* 2010; **28**:511-515.
64 Moore MJ, Zhang C, Gantman EC, Mele A, Darnell JC, Darnell RB. Mapping Argonaute and conventional RNA-binding protein interactions with RNA at single-nucleotide resolution using HITS-CLIP and CIMS analysis. *Nat Protoc* 2014; **9**:263-293.
65 Shah A, Qian Y, Weyn-Vanhentenryck SM, Zhang C. CLIP Tool Kit (CTK): a flexible and robust pipeline to analyze CLIP sequencing data. *Bioinformatics* 2017; **33**:566-567.
66 Li H, Durbin R. Fast and accurate short read alignment with

Burrows-Wheeler transform. *Bioinformatics* 2009; **25**:1754-1760.

67 Weyn-Vanhentenryck SM, Mele A, Yan Q, *et al*. HITS-CLIP and integrative modeling define the Rbfox splicing-regulatory network linked to brain development and autism. *Cell Rep* 2014; **6**:1139-1152.

68 Crooks GE, Hon G, Chandonia JM, Brenner SE. WebLogo: a sequence logo generator. *Genome Res* 2004; **14**:1188-1190.

69 Huang D W, Sherman BT, Lempicki RA. Bioinformatics enrichment tools: paths toward the comprehensive functional analysis of large gene lists. *Nucleic Acids Res* 2009; **37**:1-13.

70 Huang D W, Sherman BT, Lempicki RA. Systematic and integrative analysis of large gene lists using DAVID bioinformatics resources. *Nat Protoc* 2009; **4**:44-57.

71 Nikitin A, Egorov S, Daraselia N, Mazo I. Pathway studio-the analysis and navigation of molecular networks. *Bioinformatics* 2003; **19**:2155-2157.

72 Cline MS, Smoot M, Cerami E, *et al*. Integration of biological networks and gene expression data using Cytoscape. *Nat Protoc* 2007; **2**:2366-2382.

73 Robinson JT, Thorvaldsdottir H, Winckler W, *et al*. Integrative genomics viewer. *Nat Biotechnol* 2011; **29**:24-26.

(**Supplementary information** is linked to the online version of the paper on the *Cell Research* website.)